Determining the Isotopic Composition of Surface Water Vapor Flux From High-Frequency Observations Using Flux-Gradient and the Keeling Methods

Yongbo Hu[1, 3], Wei Xiao[1, 3], Zhongwang Wei[4], Lisa R.Welp[5], Xuefa Wen[6], Xuhui Lee[2, 1]

[1]Yale-NUIST Center on Atmospheric Environment, International Joint Laboratory on Climate and Environment Change (ILCEC), Nanjing University of Information Science and Technology, Nanjing, China.

[2]School of Forestry and Environmental Studies, Yale University, New Haven, Connecticut, USA.

[3]NUIST-Wuxi Research Institute, Wuxi, China

[4]Department of Environmental Systems Science, ETH Zurich, Zürich, Switzerland

[5]Department of Earth, Atmospheric, and Planetary Sciences, Purdue University, West Lafayette, Indiana, USA

[6]Institute of Geographic Sciences and Natural Resources Research, Chinese Academy of Sciences, Beijing, China.

Corresponding author: Xuhui Lee (xuhui.lee@yale.edu)

Key Points:

- High-frequency data was used with the Keeling method to calculate the ^{18}O isotopic composition of surface evaporation
- The Ordinary Least Squares and the York's Solution were appropriate regression methods for obtaining the Keeling intercept
- Under conditions of low vertical vapor concentration gradient, the Keeling method with OLS slightly outperformed the Flux-gradient method

Abstract

The isotopic composition of surface water vapor flux (δ_E) is a quantity frequently used to investigate the local and regional water cycle. In this study, the δ_E determined with the Keeling method was evaluated against the flux-gradient method and the Craig-Gordon model prediction. Previous studies have shown that the choice of regression fitting methods can bias the δ_E intercept results and precision of the Keeling method. Here, the Keeling method was applied to high-frequency (0.2 to 1 Hz) data measured at a cropland and a lake site to test different regression methods. Results show that the Keeling method with the York's solution (YS) and the ordinary least squares (OLS) regression produced robust estimates of δ_E when compared with the flux-gradient method. Increasing concentration range reduced the standard error of estimate but did not bring obvious improvement to the bias error for the YS and OLS regression. The Keeling result was better using data from two sampling heights than only one. There was evidence that the Keeling method with the OLS regression slightly outperformed the flux-gradient method during periods with small vertical vapor gradient. Results also show that the Keeling method with the geometric mean regression gave highly biased estimate of δ_E for the types of isotope ratio infrared spectroscopy analyzer deployed in this study. These results can inform δ_E calculations and future experimental designs.

1 Introduction

The isotopic composition of surface water vapor flux (δ_E) is a key parameter in studies of the water cycle using isotopic tracer methods. It is used for estimating lake evaporation (Gibson et al., 1993; Xiao et al., 2017), constraining local moisture recycling (Bowen et al., 2019; Gat et al., 1994; Griffis et al., 2016; Wang et al., 2016; Xiao et al., 2018), characterizing sources of moisture in the atmospheric boundary layer (Lee et al., 2007; Simonin et al., 2014; Welp et al., 2008, 2012; Zannoni et al., 2019a), and partitioning of evapotranspiration in ecosystems (Good et al., 2014, 2015; Lu et al., 2017; Sun et al., 2019; Wei et al., 2018; Wen et al., 2016). Typically, δ_E is determined with the Keeling plot method which is an application of a two-member mixing model. According to Keeling (1958), the intercept of the linear regression of the observed isotopic composition of water vapor, δ_v, against the inverse of the water vapor concentration, $1/c$, is equivalent to δ_E. The general form of this equation is

$$\delta_v = a + b(1/c) \quad (1)$$

where $\delta_E = a$.

An implicit assumption inherit in the Keeling method is that the isotopic signature of the surface water source should remain constant during the observational period. In field applications, the data used in the regression analysis are generally collected over a period of serval hours (Delattre et al., 2015; Yepez et al., 2003, 2005; Zannoni et al., 2019b). However, temporal changes in atmospheric forcings, such as relative humidity and cloudiness, can result in large short-term (minutes to hours) fluctuations in δ_E of land evapotranspiration (Dubbert & Werner, 2019; Good et al., 2012; Lee et al., 2007; Quade et al., 2019; Welp et al., 2008; Wen et

al., 2016) and open-water evaporation (Xiao et al., 2017), raising doubt about the reliability of the Keeling method (Lee et al., 2012; Pataki et al., 2003).

Another practical concern of the Keeling method is related to the choice of statistical method for the linear regression. Because the intercept of Eq (1) is obtained by extrapolation far beyond the observed data range, the result is very sensitive to how the regression parameters are obtained. A large body of papers have been published on this topic regarding the isotopic composition of terrestrial CO_2 flux (Chen et al., 2017; Kayler et al., 2010; Miller & Tans, 2003; Ogée et al., 2003; Pataki et al., 2003; Wehr & Saleska, 2017; Zobitz et al., 2006). The ordinary least squares (OLS) regression method, the most common method for estimating the regression coefficients, assumes that all measurement errors occur in the dependent variable (δ, Eq 1) and no errors exist in the independent variable (concentration, c). However, the concentration data can also suffer from measurement errors, especially if the measurement is made with gas flasks. For this reason, some researchers recommend that the geometric mean regression (GMR) or orthogonal distance regression (ODR) method should be used (Miller & Tans, 2003; Ogée et al., 2003; Pataki et al., 2003). Zobitz et al. (2006) applied the OLS and the GMR method to the CO_2 δ and concentration time series obtained with both isotope ratio mass spectroscopy (IRMS) and isotope ratio infrared spectroscopy (IRIS) instruments, and found that the difference between the two regression methods is caused by biases in the GMR regression. Chen et al. (2017) also showed that the OLS performs better than the GMR for an IRIS instrument. More recently, Wehr and Saleska (2017) introduced a general regression method, named here the York's solution (YS) method. Because the YS method takes into account error structures of the independent and dependent variables separately and also the correlation between these two types of error, the YS

method is less biased in comparison with OLS or GMR. Wehr and Saleska (2017) argued that error correlations can arise in situations where the concentration and the δ value are measured by the same instrument, such as an IRIS analyzer. However, information on the correlation pattern concerning IRIS instruments is lacking.

An alternative to the Keeling method is the flux-gradient (FG) method. Made possible by fast-responding IRIS instruments, the FG method determines δ_E from the ratio of the vertical concentration gradient of the minor to that of the major isotopologue (Griffis et al. 2005; Lee et al., 2007; Wei et al., 2018; Welp et al., 2008; Wen et al., 2016; Xiao et al., 2017). The molar ratio of the $H_2{}^{18}O$ flux to the $H_2{}^{16}O$ flux is given by

$$R = (c_2^i - c_1^i)/(c_2 - c_1) \quad (2)$$

where c^i and c denote the hourly mean molar mixing ratio of $H_2{}^{18}O$ and $H_2{}^{16}O$, respectively, and subscripts 1 and 2 denote the lower and the upper measurement level, respectively. The molar flux ratio R is then converted to the δ scale to give δ_E. In a typical application, an IRIS instrument samples water vapor sequentially and at a high frequency (e.g., 1 Hz) between two heights above the surface, and the gradient ratio is calculated from the high frequency data. Because a measurement period can be as short as 30 to 60 minutes in practice, this method can capture dynamic variations in δ_E. However, the FG method becomes very noisy because of errors arising from division by small numbers. For this reason, the result is unreliable when the vertical vapor concentration difference $c_2 - c_1$ small in magnitude, for example, under conditions of high turbulent mixing.

In this study, we evaluate a hybrid approach that combines the Keeling method with the high frequency data originally intended for FG calculation. The idea of applying the Keeling method to high frequency time series was first proposed by Bowling et al. (1999) before the emergence of the IRIS technology and was later tested with CO_2 isotope data collected with an IRIS instrument (Griffis et al., 2004). Because the data are collected at a high frequency, the sample size is large (typically > 700 in one hour), effectively increasing the variability in the observed water vapor concentration and decreasing the uncertainty of parameter estimation (Good et al., 2012). By restricting the regression to a short period (hourly), time variations of the source isotopic signature are not a major concern. In this paper, we are interested in whether this hybrid Keeling method can yield more robust estimates of δ_E than the FG method under low vertical vapor gradient conditions by incorporating information on both vertical variations and temporal variations in the vapor concentration and the $\delta^{18}O$.

Our study builds on the work of Wehr and Saleska (2017) and Good et al. (2012). Wehr and Salesak (2017) have demostrated the generality of the YS model for finding the best-fit straight line. Their discusison is based on synthetic datasets generated for CO_2 isotopes. In the present study, we extend their work to water vapor isotopes and to real data collected by two common IRIS instruments at two contrasting types of surface (a cropland and a lake). Good et al. (2012) compared uncertainties in the assessment of the isotopic composition of surface evapotranspiration among several methods (Keeling, flux-gradient and eddy covariance). Their focus is primarily on random errors of parameter estimation. Here we also examine systematic biases. The specific objectives of this study are (1) to characterize the error structures of IRIS instruments for the Keeling method involving the YS regression model, (2) to compare the

sysematic bias errors of the OLS, GMR and YS regression methods, and (3) to evaluate the performance of the Keeling method and the FG method under conditions of low vertical gradient of water vapor concentration.

While random errors of the regression coefficients can be obtained with statistical methods (Good et al., 2012; Zobitz et al., 2006), assessment of bias errors requires that the true isotopic signal of the surface flux be known. In the case of a pure C_3 ecosystem, the ^{13}C composition of the respiration CO_2 flux is reasonably well constrained, and the expected ^{13}C signal (e. g., about -25‰; Wehr et al., 2016) can be used to benchmark the bias errors of regression models and regression methods (Chen et al., 2017; Zobitz et al., 2006). In other situations, the isotopic composition of the surface flux is not known *a priori*. To overcome this problem, some researchers used synthetic data that combines a hypothetical flux isotopic signal with random variations superimposed on the concentration and the δ variable (Chen et al., 2017; Kayler et al., 2010; Vardag et al., 2016; Wehr & Saleska, 2017; Zobitz et al., 2006). In this study, we assume that the flux-gradient method provides an unbiased estimate of δ_E under high vertical vapor gradient conditions and can be used to evaluate bias errors associated with the Keeling method. Additionally, for our lake site, the "true" δ_E is also obtained from the Craig-Gordon model of the isotopic composition of open-water evaporation (Craig & Gordon, 1965) with a locally calibrated kinetic fractionation factor (Xiao et al., 2017).

2 Materials and Methods

2.1 Sites and instruments

The datasets used in this study were obtained in two field experiments. The first experiment was conducted in an irrigated maize field in Zhangye, Gansu Province, in Northwest China (38° 51′ N, 100° 22′ E) in 2012 (Wen et al., 2016). The fetch was larger than 200 m in all wind directions. Climate in Zhangye is arid with an annual mean temperature of 7.4 °C and mean annual precipitation of 129 mm. The H_2O, HDO and $H_2{}^{18}O$ concentrations were measured at two heights (0.5 m and 1.5 m) above the canopy with an IRIS water vapor isotope analyzer (Model L1102-i, Picarro Inc. CA, USA) at 0.2 Hz. The hourly precision for the vapor $\delta^{18}O$ is ~0.1‰ (Wen et al., 2012b). Switching between the two intake heights occurred every 2 min. The last 8 datapoints after each switching, corresponding to the last 40 seconds, were saved for the analysis. The analyzer was calibrated in-situ with a liquid vaporization module (Picarro Inc) and a CTC Analytics Prep and Load liquid autosampler (LEAP Technologies, Carrboro, NC, USA) using a single liquid water standard with a $\delta^{18}O$ value of -14.29‰. There were 3 concentrations of calibration vapor, each measured for 25 min. After each calibration vapor, three hours were spent on the measurement of ambient air. A linear interpolation between two consecutive calibration cycles was used to obtain the span for correcting the ambient air measurement (Huang & Wen, 2014; Wen et al., 2008, 2012a).

The other experiment was conducted at Meiliangwan (MLW, 31° 15' N, 120° 13′ E) in the northern part of Lake Taihu as part of the Taihu Eddy Flux Network (Lee et al., 2014) between August 2012 and September 2016. Lake Taihu is located in the Yangtze River Delta, Eastern China. The annual mean temperature is 16.2 °C and the mean annual precipitation is 1,120 mm.

The H_2O, HDO and $H_2{}^{18}O$ concentrations were measured at two heights (1.1 m and 3.5 m) above the water surface with an IRIS water vapor isotope analyzer (Model 911-0004; Los Gatos Research, Mountain View, CA, USA) at 1 Hz. The 2-min precision of this instrument for the vapor $\delta^{18}O$ is 0.2‰ (Xiao et al., 2017). Switching between the two intakes occurred every 30 s, with the last 15 datapoints, corresponding to the last 15 seconds, used for gradient calculations. The measurement site was located at a linear distance of 250 m from the northern shore. To minimize land influence on the measurement, we restricted our analysis to the data collated in the wind direction sector of 140° to 315°, corresponding to a fetch of 8 to 50 km. The in-situ calibration vapor was generated by a water vapor isotope standard source (Model 908-0003-9002; Los Gatos Research). The calibration was performed every 3 h. Each calibration cycle consisted of 5 concentrations and lasted for 30 min in total. Other details of this experiment can be found in Xiao et al. (2017).

2.2 Regression methods

In this study, three regression methods were used in the Keeling method to obtain the intercept of a linear equation $y = a + bx$: ordinary least squares regression (OLS), geometric mean regression (GMR), and York's solution (YS). The OLS seeks to minimize the sum of the squared residuals between the expected values of the dependent variable *y* and the data points. The result is unbiased only if errors in the independent variable *x* are negligible and errors in the dependent variable *y* are constant. The slope *b* and intercept *a* can be expressed as,

$$b_{\mathrm{OLS}} = \frac{\sum(x_{\mathrm{i}}-\overline{x})(y_{\mathrm{i}}-\overline{y})}{\sum(x_{\mathrm{i}}-\overline{x})^2} \quad (3)$$

$$a_{\mathrm{OLS}} = \overline{y} - b_{\mathrm{OLS}}\overline{x} \quad (4)$$

where x_i and y_i are observed values, and $\overline{x}$ and $\overline{y}$ are the corresponding mean values. The standard error of slope b obtained with OLS, σ_b, can be expressed as

$$\sigma_{bOLS} = \sqrt{\frac{\sum(y_i - \hat{y}_i)^2}{(n-2)\sum(x_i - \bar{x})^2}} \quad (5)$$

and the standard error of intercept obtained with OLS, σ_a, can be expressed as

$$\sigma_{aOLS} = \sqrt{\frac{\sigma_b{}^2 \sum x_i{}^2}{n}} \quad (6)$$

where n is the number of datapoints and $\hat{y}_i$ is the expectation values of y_i, $\hat{y}_i = b_{OLS}x_i + a_{OLS}$.

The GMR seeks to minimize both the vertical (dependent variable, y) and horizontal (independent, x) residuals. The result is unbiased only when the error in x divided by the variance of x is equal to the error in y divided by the variation of y (Kermack & Haldane, 1950). The slope b and intercept a can be expressed as,

$$b_{GMR} = \sqrt{b_{yx}\frac{1}{b_{xy}}} \quad (7)$$

$$a_{GMR} = \overline{y} - b_{GMR}\overline{x} \quad (8)$$

where both b_{yx} and b_{xy} are obtained from the OLS, but they have different independents: b_{yx} is the slope when x is chosen as the independent variable, and b_{xy} is the slope when y is chosen as the independent variable. Eqs (5) and (6) can also be used to obtained σ_b and σ_a of the GMR, where the expected y_i is obtained with the GMR regression coefficients (Eqs 7 and 8).

There is a relationship between the slope obtained with GMR and OLS,

$$b_{GMR} = \frac{b_{OLS}}{|r|} \quad (9)$$

where r is Pearson's correlation coefficient between x and y.

Generally, both x and y have measurement errors, and these errors may also be correlated. While neither the OLS nor the GMR method accounts for the error correlation, the YS method takes the correlation between errors in x and errors in y into account to obtain a best-fit straight line (York, 1966, 1969; York et al., 2004). The slope and intercept from YS can be expressed as,

$$b_{\mathrm{YS}} = \frac{\sum W_{\mathrm{i}}\beta_{\mathrm{i}}(x_{\mathrm{i}}-\overline{x})}{\sum W_{\mathrm{i}}\beta_{\mathrm{i}}(y_{\mathrm{i}}-\overline{y})} \tag{10}$$

$$a_{\mathrm{YS}} = \overline{y} - b_{\mathrm{YS}}\overline{x} \tag{11}$$

where $\overline{x}$ and $\overline{y}$ are weighted means of x and y

$$\overline{x} = \frac{\sum W_{\mathrm{i}}x_{\mathrm{i}}}{\sum W_{\mathrm{i}}}, \overline{y} = \frac{\sum W_{\mathrm{i}}y_{\mathrm{i}}}{\sum W_{\mathrm{i}}} \tag{12}$$

and β_{i}, an intermediate variable, is given by

$$\beta_{\mathrm{i}} = W_{\mathrm{i}}[\frac{x_{\mathrm{i}}-\overline{x}}{\omega(y_{\mathrm{i}})} + \frac{b(y_{\mathrm{i}}-\overline{y})}{\omega(x_{\mathrm{i}})} - \big(b(x_{\mathrm{i}}-\overline{x}) + (y_{\mathrm{i}}-\overline{y})\big)\frac{r_{\mathrm{i}}}{\sqrt{\omega(x_{\mathrm{i}})\omega(y_{\mathrm{i}})}}] \tag{13}$$

In Eq (13), b is an initial guess of the slope which can be obtained from the OLS regression, r_{i} is correlation between errors in x_{i} and errors in y_{i}, and $\omega(x_{\mathrm{i}})$ and $\omega(x_{\mathrm{i}})$ are weights of x_{i} and y_{i} given by

$$\omega(x_{\mathrm{i}}) = \frac{1}{\sigma^2(x_{\mathrm{i}})}, \omega(y_{\mathrm{i}}) = \frac{1}{\sigma^2(y_{\mathrm{i}})} \tag{14}$$

where $\sigma(x_{\mathrm{i}})$ and $\sigma(y_{\mathrm{i}})$ are errors in horizontal ($1/c$) and vertical ($\delta^{18}O$) coordinates at the ith data point. The intermediate variable W_{i} in Eqs (11) and (12), or the weight of ith point, is given by

$$W_{\mathrm{i}} = \frac{\omega(x_{\mathrm{i}})\omega(y_{\mathrm{i}})}{\omega(x_{\mathrm{i}})+b^2\omega(y_{\mathrm{i}})-2br_i\sqrt{\omega(x_{\mathrm{i}})\omega(y_{\mathrm{i}})}} \tag{15}$$

Typically, the number of iterations is less than 10 from the initial to the final slope value. The standard error of slope obtained with YS can be expressed as

$$\sigma_{\mathrm{bYS}} = \sqrt{\frac{1}{\sum W_i(X_i-\bar{X})^2}} \tag{16}$$

and the standard error of intercept obtained with YS can be expressed as

$$\sigma_{\mathrm{aYS}} = \sqrt{{\sigma_{\mathrm{b}}}^2 \overline{X}^2 + \frac{1}{\sum W_{\mathrm{i}}}} \tag{17}$$

where $X_i = \overline{x} + \beta_i$ and $\overline{X} = \frac{\sum W_{\mathrm{i}} X_{\mathrm{i}}}{\sum W_{\mathrm{i}}}$.

2.3 Characterization of error structures

The error parameters in the YS method, $\sigma(x_{\mathrm{i}})$, $\sigma(y_{\mathrm{i}})$ and r_{i}, for Lake Taihu were determined with the field calibration data. A calibration cycle consisted of 5 concentrations, each lasting for 6 min. An example of the calibration stepping is given by Xiao et al. (2017; their Figure 4). The standard deviation of $1/c$, the standard deviation of $\delta^{18}O$ and the correlation coefficient between $1/c$ and $\delta^{18}O$ were calculated for each concentration interval. We assume that these variations originated purely from measurement errors. The data during transition from one concentration level to the next were excluded from the calculation.

For Zhangye, the field calibration data cannot be used to characterize the measurement errors because the concentration of the water vapor generated by the liquid vaporization module was not stable during the calibration phase. To obtain the error parameters, we carried out additional measurements in the laboratory using the same IRIS water vapor isotope analyzer deployed in the field. The analyzer was configured to measure the water vapor concentration and the isotopic composition of a water vapor stream generated by a standard delivery module (Model A0101; Picarro Inc.). The delivery module was fed with liquid water of known $\delta^{18}O$ value (-9.17‰). Each measurement cycle included 3 water vapor concentrations and lasted for 1 h. A total of 141 measurement cycles were performed, with the vapor concentration ranging from

7,900 ppm to 27,690 ppm. The same method used for Lake Taihu was deployed to obtain the error parameters.

2.4 Data processing

The high-frequency IRIS data were used to calculate δ_E for each hourly observation interval using the three regression methods described above. Each observation, including data obtained for both measurement heights, consisted of about 200 and 1,800 data points for Zhangye and Lake Taihu, respectively. Figure 1 shows the time series of the water vapor mixing ratio and the calibrated vapor $\delta^{18}O$ from a typical observation period at Lake Taihu, and Figure 2 shows the corresponding linear regression plot. The δ_E estimated from the Keeling method was then compared with the δ_E obtained from the FG method. Additionally, at Lake Taihu, comparison was also made with the Craig-Gordon model calculation of the lake evaporation delta using a locally-tuned kinetic fractionation factor (Xiao et al., 2017).

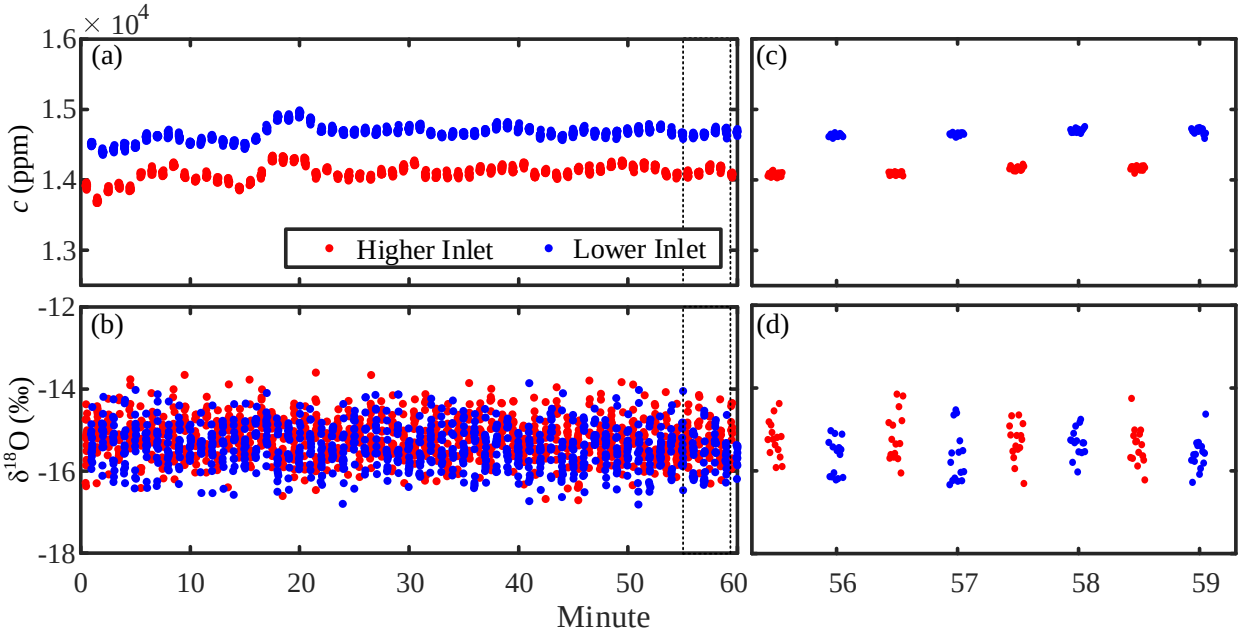

Figure 1. Temporal variation of H_2O mixing ratio (a) and $\delta^{18}O$ (b) at the lower inlet (blue dots) and higher inlet (red dots) at Lake Taihu between 16:00 and 17:00 local time on October. 22nd, 2014. Panels c and d are the corresponding zoom-in plot of the dotted box in panels a and b.

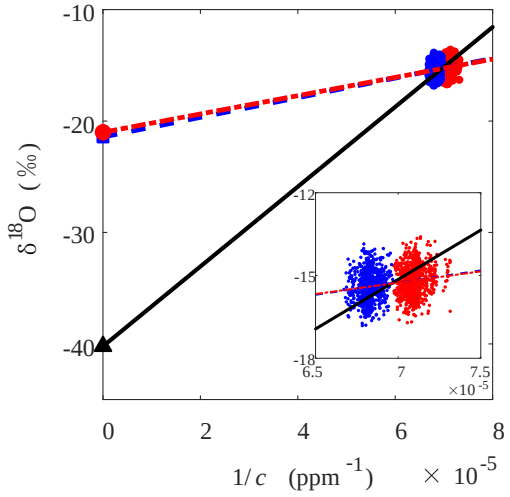

Figure 2. An illustration of the three regression methods applied to the data in Figure 1. YS: red-dot-dashed line; OLS: blue-dashed line; GMR: black-solid line; blue dots: observations at lower inlets; red dots: observations at higher inlet. In this hour, the δ_E obtained from the FG method is -21.0‰, with a standard deviation 4.78‰.

Three criteria were used to screen the data. The FG method becomes noisy at times of small vertical concentration gradients. To ensure a robust comparison, we restricted most of our analysis to observations whose hourly mean vertical vapor concentration difference between the two measurement heights is larger than 200 ppm in magnitude. About 2/3 of the 3,026 and 1,622 valid observations satisfy this criterion at Zhangye and Lake Taihu, respectively. The second criterion was the standard deviation of δ_E calculated by the FG method; we used a threshold value of 20‰. The third criterion required that the *P* value obtained from the Keeling method be smaller than 0.05 to ensure that the relationship between $1/c$ and $\delta^{18}O$ passes the significance test

(Unger et al., 2010). A total of 1,084 and 817 hourly observations remained for Zhangye and Lake Taihu, respectively, after the data screening.

3 Results and Discussion

3.1 Error structures of the vapor concentration and the isotope composition

The relationships between the water vapor concentration and the standard deviation of $1/c$, the standard deviation of $\delta^{18}O$ and correlation coefficient r, established with the data collected during the instrument calibration cycles, are shown in Figure 3. Unsurprisingly, the standard deviation of $1/c$ was greater at lower concentrations, with the Picarro analyzer (used at Zhangye) and the LGR analyzer (used at Lake Taihu) giving similar performance. The standard deviation of $1/c$ was 4.02×10^{-7} and 3.37×10^{-7} ppm^{-1} at a water vapor concentration of 10,000 ppm and 1.29×10^{-7} and 9.40×10^{-8} ppm^{-1} at a concentration of about 30,000 ppm, for Zhangye and Lake Taihu, respectively. The standard deviation of $\delta^{18}O$ showed opposite trends for the two sites. At Zhangye, the standard deviation of $\delta^{18}O$ was relatively constant at concentrations lower than about 20,000 ppm and increased with increasing concentration beyond this threshold. At Lake Taihu, the standard deviation of $\delta^{18}O$ showed a general decreasing trend with increasing concentration. At Zhangye, the correlation between measurement errors in $1/c$ and in $\delta^{18}O$ was slightly positive at low concentrations (~10,000 ppm) and varied around zero at high concentrations (~25,000 ppm). At Lake Taihu, the error correlation was mostly positive and did not seems to depend on the vapor concentration.

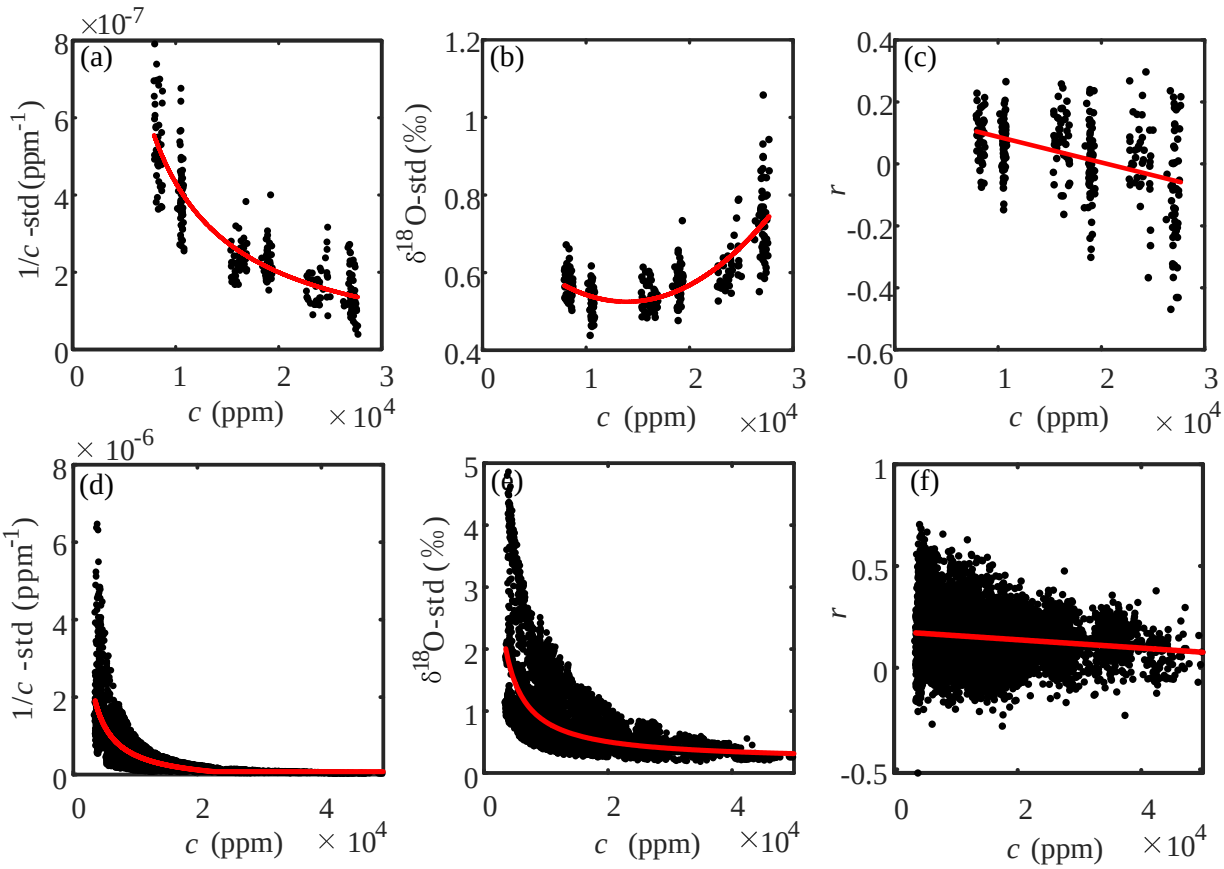

Figure 3. Relationships between water vapor concentration and errors in 1/c, errors in δ^{18}O and correlation coefficient between errors in δ^{18}O and errors in 1/c for Zhangye (a, b and c) and Lake Taihu (d, e and f). The solid red line in each panel indicates the regression fit, with the regression equation given in Supplementary Table S1.

Results of regression fitting to the data shown in Figure 3 are summarized in Supplementary Table S1.These regression equations were used to determine parameters $\sigma(x_i)$, $\sigma(y_i)$ and r_i in Eqs (14) and (15) as functions of c_i. For example, the error in the vertical axis (δ^{18}O) at time i is given as $\sigma(y_i) = f_y(c_i)$, where f_y is the regression fitting equation, and c_i is the measured concentration at time i. Our method for determining these error parameters differs from that used by Wher and Saleska (2017). In their study, errors in the horizontal and the

vertical axis are set to prescribed hourly instrument precisions and the correlation between these two errors is set to zero. Compared with the precision of the instrument, the parameters $\sigma(x_i)$ and $\sigma(y_i)$ in this study were larger because of random errors at high sampling frequencies and were more realistic representations of the actual measurement errors in field conditions.

3.2 Comparison of regression methods

Figure 4 compares δ_E determined with the FG method and the Keeling intercept using the three regression methods. Each data point represents one hourly δ_E calculated using data from two measurement heights above the surface. The δ_E values based on the YS and OLS regression method were comparable with the FG results. The two methods yielded similar mean bias errors (YS: 1.08‰; OLS: 0.92‰) at Zhangye, and OLS slightly outperforms YS at Lake Taihu, with a mean bias 1.05‰ for YS and 0.14‰ for OLS. In contrast, the GMR results were rather poor, with large mean bias errors (6.97 and -1.66‰ for Zhangye and Lake Taihu, respectively) and large scatters (low linear correlation *R* values).

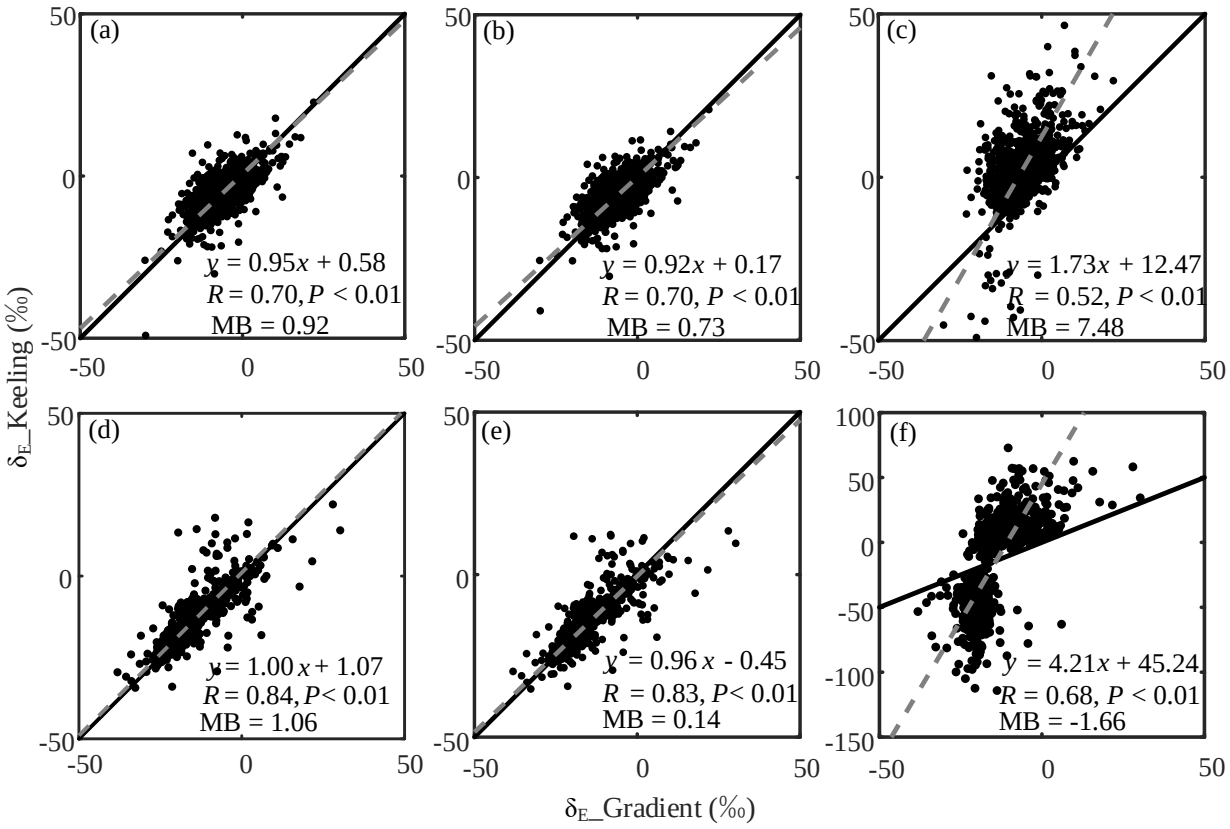

Figure 4. Comparison of the evaporation isotopic signature δ_E obtained with the flux-gradient method and with the Keeling method for Zhangye (a, b and c) and Lake Taihu (d, e and f). Panels a and d: YS regression; panels b and e: OLS regression; panels c and f: GMR regression. Solid black lines are the 1:1 comparison and the regression equation is listed for each panel along with the correlation coefficient, *R*, significance, *P*, and mean bias (MB, ‰).

An implicit assumption of GMR is that the normalized errors in *x* and *y* are equal (Kermack & Haldane, 1950). This assumption is not satisfied here. Table 1 shows the mean errors in $1/c$ and $\delta^{18}O$, and these errors normalized by the ranges of $1/c$ and $\delta^{18}O$ for three levels of water vapor concentration. Here the range of a variable is defined as the difference between the maximum and the minimum value of the high-frequency data in a given 60-min observational period. Errors existed both in the horizontal coordinate $1/c$ and the vertical

coordinate $\delta^{18}O$. The normalized error in $\delta^{18}O$ was, however, much larger than the normalized error in $1/c$, by a factor of 6 to 10 at Zhangye and of 3 to 7 at Lake Taihu.

Table 1. Measurement errors in three quantiles of water vapor concentration. Errors are calculated as one standard deviation of high frequency data (0.2 Hz at Zhangye and 1 Hz at Lake Taihu). Here c and $\delta^{18}O$ denotes water vapor concentration and vapor ^{18}O isotope ratio, respectively.

Quantile	Mean c ppm	Error in $1/c$ ppm^{-1}	Error in $\delta^{18}O$ ‰	c range ppm	$\delta^{18}O$ range ‰	$1/c$ range ppm^{-1}	Error in $1/c$ / ($1/c$ range)	Error in $\delta^{18}O$ / ($\delta^{18}O$ range)
				Zhangye				
0 - 25	7688	5.86×10^{-7}	0.57	1856	3.48	3.64×10^{-5}	0.016	0.16
25 - 75	12984	3.32×10^{-7}	0.53	2659	3.50	1.65×10^{-5}	0.020	0.15
75 - 100	18930	2.16×10^{-7}	0.55	3566	3.95	1.02×10^{-5}	0.021	0.14
				Lake Taihu				
0 - 25	9171	5.73×10^{-7}	0.88	1262	7.43	1.73×10^{-5}	0.033	0.12
25 - 75	21213	1.02×10^{-7}	0.49	1697	3.29	4.27×10^{-6}	0.024	0.15
75 - 100	30879	7.87×10^{-8}	0.40	2232	3.11	2.35×10^{-6}	0.033	0.13

Strictly, the OLS regression is unbiased only if no errors exist in $1/c$. But because the normalized error in $1/c$ was several times smaller than the normalized error in $\delta^{18}O$, the OLS regression yielded robust results. Similar conclusions have been reported by Zobitz et al. (2006), Chen et al. (2017) and Wehr and Saleska (2017) for carbon isotopes of CO_2. In their studies, the relative error in $\delta^{13}C$ measurements is larger than relative error in CO_2 concentration measurements, so the OLS provides better results than the GMR. Wehr and Saleska (2017) cautioned that OLS will introduce obvious bias if the relative error in CO_2 concentration measurements is large or the relative error in $\delta^{13}C$ measurements is small.

Zobitz et al. (2006) concluded that the bias error associated with the GMR is mathematical in nature. Pataki et al. (2003) reported that the GMR intercept is systematically more negative than the OLS intercept when applied to the calculation of the ^{13}C composition of ecosystem respiration. In our study, the δ_E from the GMR could be biased either high or low. At Zhangye, almost all the datapoints were located above the 1:1 line (Figure 4c), indicating a high bias, while at Lake Taihu, the bias was mostly positive when the δ_E from the Keeling method with the GMR was greater than -15‰ and mostly negative when δ_E was less than -15‰.

3.3 Dependence on water vapor concentration range

It is well established that increasing the CO_2 concentration range will reduce the standard error as well as the systematic bias associated with the ^{13}C signature of the respiration CO_2 flux inferred from the Keeling method. This is true for observations made with flasks (Pataki et al., 2003; Zobitz et al., 2006) and IRIS instruments (Chen et al., 2017; Zobitz et al., 2006) and for synthetic CO_2 datasets (Kaylor et al., 2010; Wher & Saleska, 2017). Whether these findings can

379 be extended to water vapor observations is not known. Here this range effect is examined from
380 three perspectives. First, we find that the standard error of the δ_E estimate showed strong
381 dependence on the water vapor concentration range, the maximum minus the minimum water
382 vapor concentration during each hourly observation (Figure 5 and Supplement Table S2). At both
383 sites, the uncertainty of δ_E decreased with increasing concentration range. Although all the three
384 regression methods yielded a linear relationship on the log-log scale, the range dependence of the
385 YS method (Figure 5a and 5d) was much tighter than those of the OLS (Figure 5b and 5e) and
386 the GMR method (Figure 5c and 5f). So from the standpoint of predicting the uncertainty of
387 individual observations, YS was better than the other two regression methods. The log-log
388 relationship was also reported by Good et al. (2012) for water vapor. Chen et al. (2017)
389 compared the OLS and the GMR methods using data obtained with an IRIS CO_2 analyzer and
390 found that the OLS method produces smaller standard errors than the GMR method.

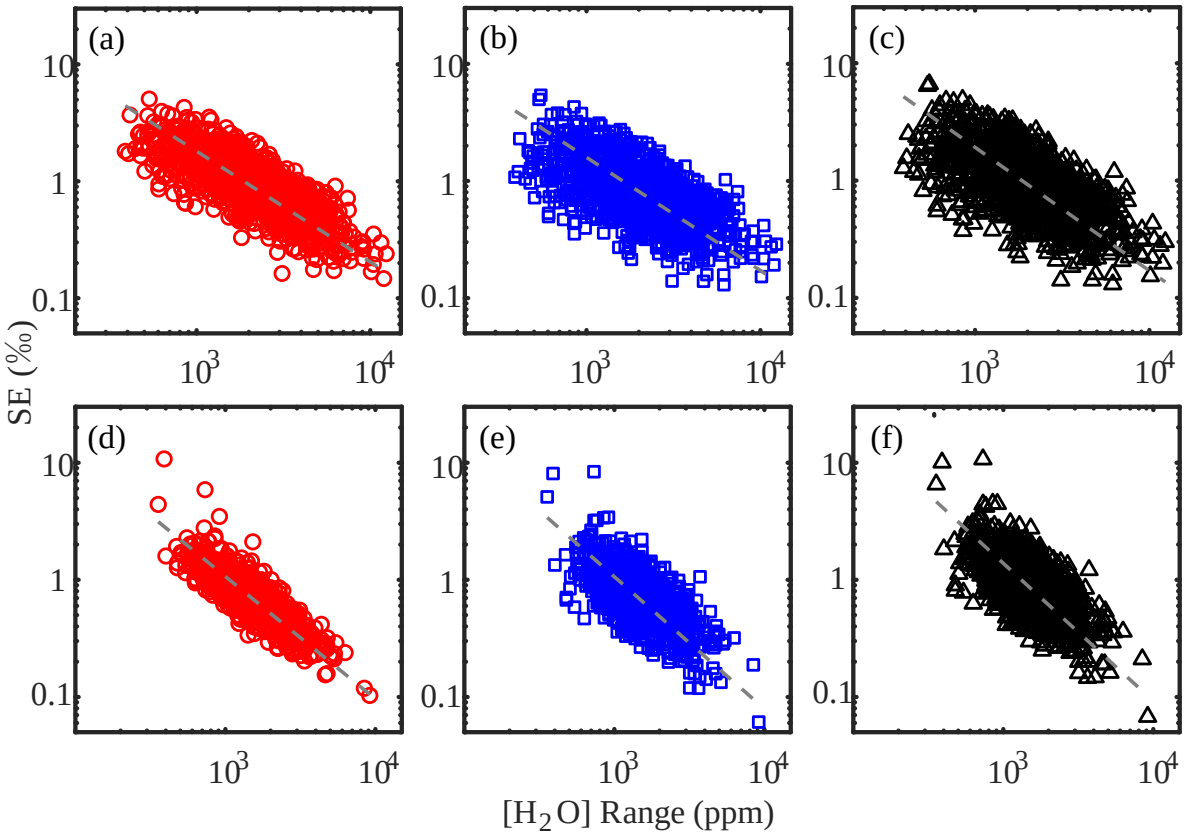

Figure 5. Relationships between the water vapor concentration range and the standard error of the Keeling method with the YS (a and d), the OLS (b and e) and the GMR regression (c and f) based on the two-height data at Zhangye (a, b and c) and Lake Taihu (d, e and f). Also shown are the best fit lines, with the regression statistics given in Supplemenatry Table S2.

Second, the bias errors associated with the YS and OLS regression did not show obvious dependence on concentration range (Figure 6). In other words, a larger concentration range helped to reduce random errors of the parameter estimate of these two methods but did not brings obvious improvement to their systematic bias errors. For comparison, the GMR estimate of δ_E was biased high at Zhangye, in reference to the δ_E obtained with the FG method, and the systematic bias increased with decreasing concentration range (Figure 6a). At Lake Taihu, the

GMR result was biased high at high concentration ranges and biased low at low ranges (Figure 6b).

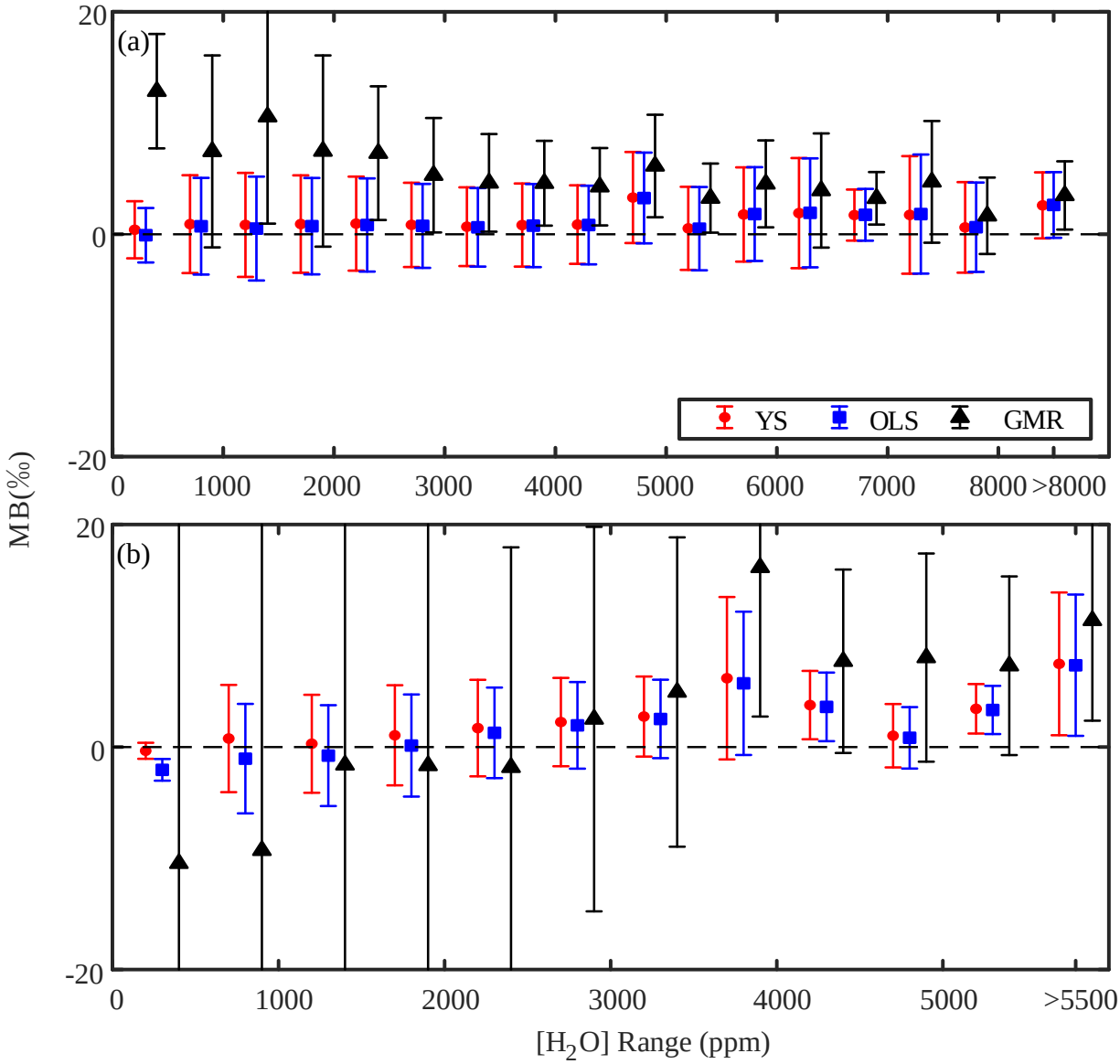

Figure 6. Mean bias of the evaporation isotope ratio (Keeling estimate minus the FG value) as a function of the water vapor concentration range at Zhangye (a) and Lake Taihu (b). Error bars are standard deviation of the bias for each bin.

Third, the correlation between $1/c$ and $\delta^{18}O$ generally improved with increasing concentration range (Figure 7). This correlation pattern explains in part why the systematic bias error of the GMR intercept was larger at lower concentration ranges (Figure 6). Figure 8 shows that the systematic bias error of the GMR method was sensitive to the sign of the correlation, showing positive biases at times of negative correlation and vice versa. At the Zhangye cropland, the correlation between $\delta^{18}O$ and the inverse of the vapor concentration was negative for 98% of the observations (Figure 8a), and the GMR bias error was mostly positive (Figures 4c and 6a). At Lake Taihu, the correlation was negative for 53% and positive for 47% of the observations (Figure 8b), explaining the bifurcation pattern shown in the 1:1 plot (Figure 4f). According to Eq (9), the slope b_{GMR} of the GMR regression is larger in magnitude than the slope b_{OLS} of the OLS regression. In cases of positive R, the regression slope is positive and a larger positive slope leads to a negative bias of the GMR intercept. Conversely, in cases of negative R, a more negative slope leads to a positive bias of the intercept.

In the CO_2 isotopic studies, increasing the absolute correlation coefficient is also an effective way to decrease the bias of the result obtained by the GMR method (Bowling et al., 2005; Chen et al., 2017; Zobitz et al., 2006). In these studies, the correlation between $\delta^{13}C$ and the inverse of the CO_2 concentration is generally positive, so the bias in the GMR intercept is generally negative (Pataki et al., 2003).

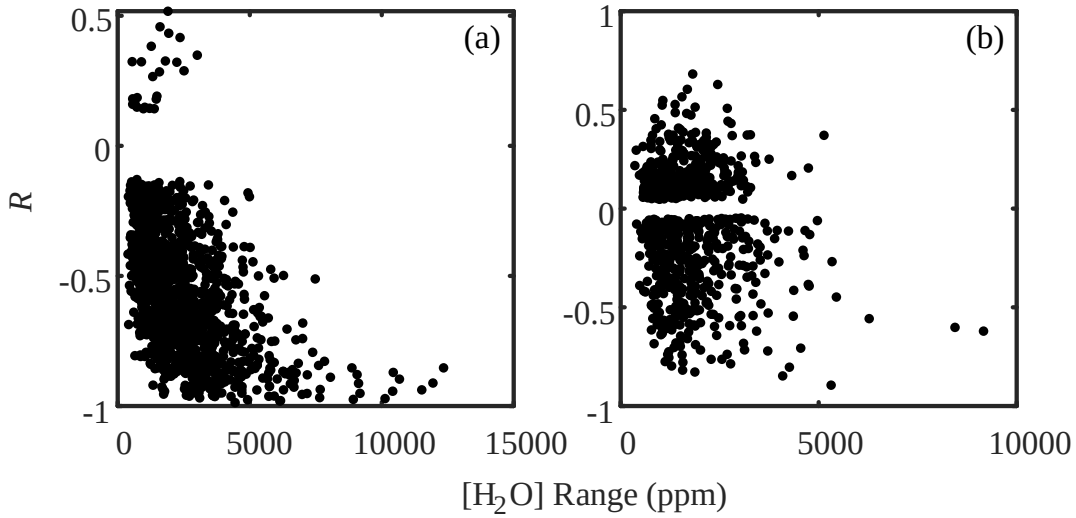

Figure 7. Relationship between the Pearson's correlation coefficient (between the inverse of the vapor concentration and the vapor δ value) and H_2O range at Zhangye (a) and Lake Taihu (b). Each datapoint represents one hourly observation including data from two measurement heights. All the observations shown here passed the sigificance test ($P < 0.05$).

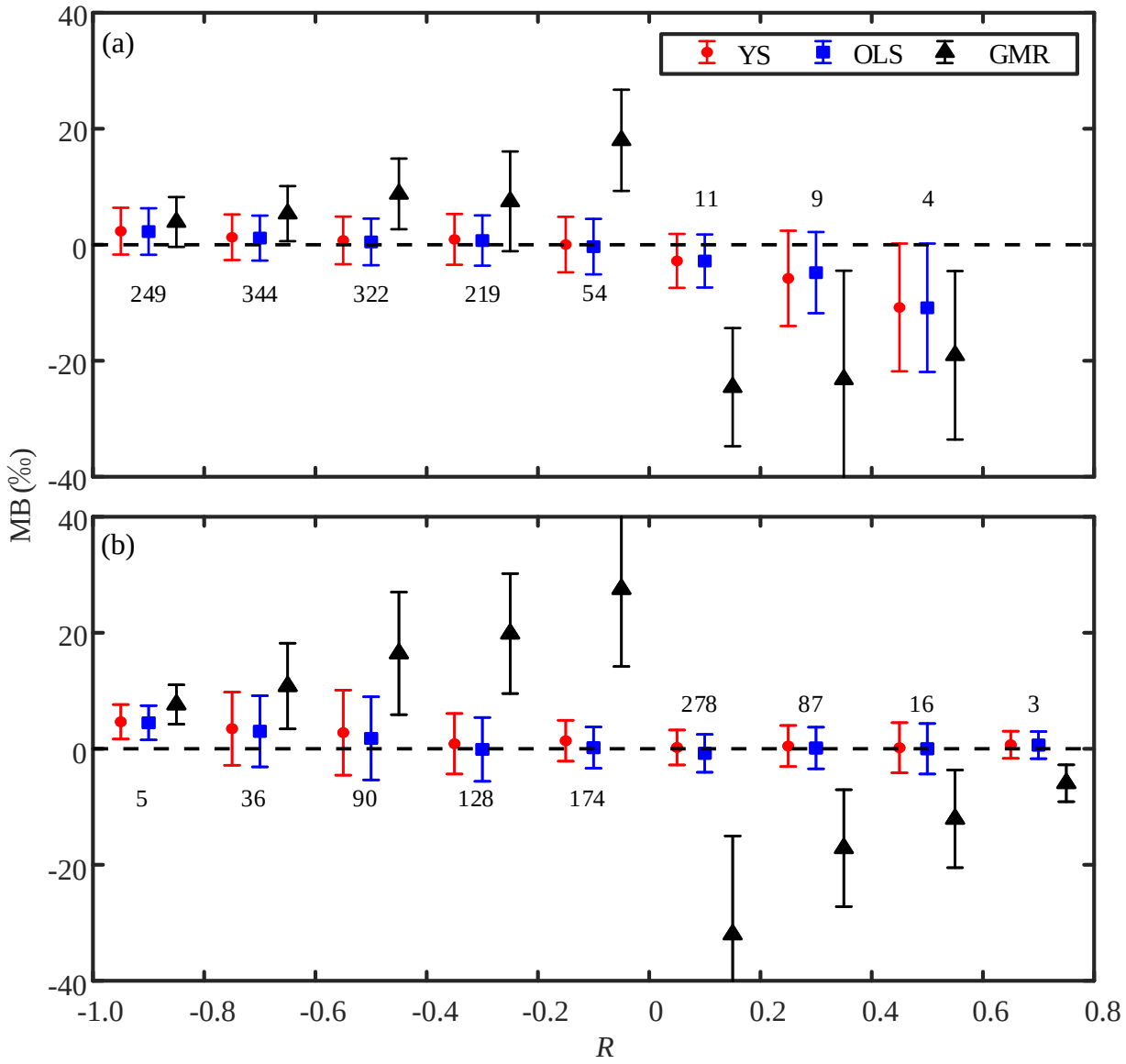

Figure 8. Mean bias of the evaporation isotope ratio δ_E (Keeling estimate minus FG value) as a function of the correlation coefficient *R* between the inverse of the concentration and the vapor δ value at Zhangye (a) and Lake Taihu (b). All the observations used here for bin averaging passed the 0.05 sigificance test. Also shown is the number of observations for each bin.

At Lake Taihu, the bias errors of the OLS and YS methods were not sensitive to the correlation strength. At Zhangye, their errors were not sensitive to the correlation strength if the

correlation is negative. If the correlation is positive, the OLS and YS showed similar high biases of -4.90‰ to -5.25‰ (bin averages), but that may be because the number of samples used for bin averaging was very small (< 12 datapoints per bin) for Zhangye.

3.4 Results from single-height data

In this section, we evaluate the three regression models using high frequency data collected at a single height. Logistically, it is much easier to measure the water vapor isotopic composition at a single height than at multiple heights involving valve switching. Indeed, the great majority of the published IRIS water vapor isotope measurements was conducted with a single-height configuration (Fiorella et al., 2018; Wei et al., 2019; Yao et al., 2018; Zannoni et al., 2019a). Figure 9 is based on the high-frequency data collected at the lower measurement height. All the three regression models performed less well when only data from the lower height were used than when data from both heights were used to determine the regression (Figure 4). For example, at Lake Taihu, the mean bias error of the OLS changed to -2.82‰ (Figure 9e) from 0.14‰ (Figure 4e) and the correlation between the Keeling and the FG method was reduced to 0.26 from 0.83. Use of the data collected at the upper height yielded essentially the same conclusion (Supplementary Figure S1).

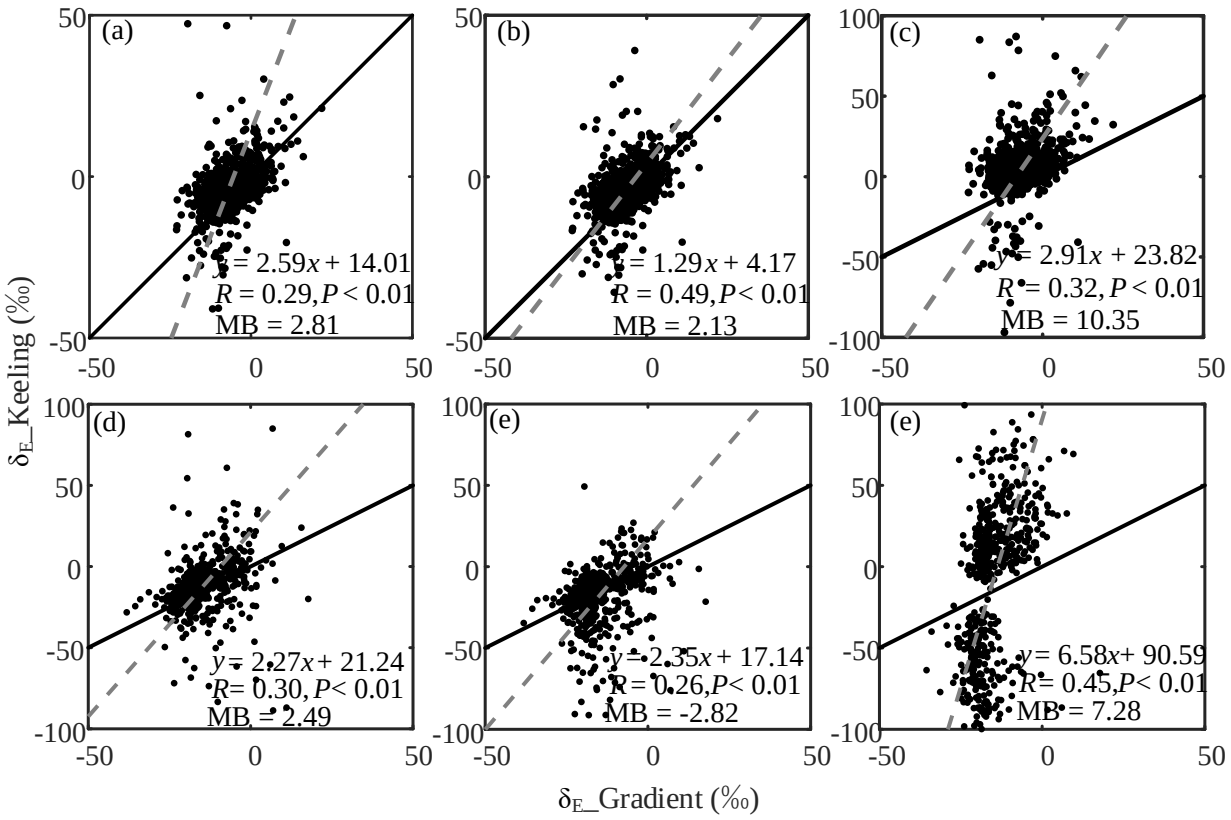

Figure 9. Same as Figure 4 except that only the data observed at the lower measurement inlet was used for the Keeling analysis.

The deteriorated performance in Figure 9 resulted in part from a reduced sample size and from a narrower concentration range. The sample size was halved when only one-height measurement was used. In the example shown in Figure 1, the concentration range is 673 and 1,318 ppm for the data at the lower height and for both heights, respectively. The mean concentration ranges were 2,063 and 1,137 ppm for Zhangye and Lake Taihu, respectively, for the data shown in Figure 9, whereas the mean ranges were larger, at 2,534 and 1,712 ppm for Zhangye and Lake Taihu, respectively, in Figure 4. The standard error of the intercept was larger with one-height measurements than with two-height measurements (Supplementary Figure S2). Similarly, Good et al. (2012) reported that the uncertainty of the isotopic composition of

evapotranspiration associated with high-frequency time series measured at a single height is 25% larger than with a combined use of time series measured at multiple heights.

While the systematic biases of the GMR regression in Figure 9 (panels c and f) are mathematical in nature (as in Figure 4 panels c and f), the biases of the OLS and the YS regression here may be related to footprint influences, especially at Zhangye where the fetch was short (about 200 m). At Zhangye, 70% and 68% of the data points lay above the 1:1 line (Figure 9 panels a and b), and the mean biases were 2.81‰ and 2.13‰, for YS and OLS, respectively. Griffis et al. (2007) found that the Keeling plot method with one-height data yields lower estimates of the ^{13}C composition of ecosystem respiration of a C_4 crop than the FG method. They attributed this difference to a footprint mismatch: the single-height concentration has a much larger source area and is therefore more influenced by the surrounding C_3 crops, than the FG data. Interestingly, Good et al. (2012) also found higher δ_E values with the Keeling method using single-height data than using data from multiple heights (mean difference about 16‰ for ^{18}O, black triangles in their Figure 8).

3.5 Performances under low vertical vapor gradient conditions

To determine whether the Keeling method gives a more robust estimate of δ_E than the FG method under low gradient conditions, we used the Craig-Gordon model as a reference to evaluate their performance for Lake Taihu (Figure 10). Low gradient conditions tended to occur at times of low evaporation flux at Lake Taihu and could occur at times of both low and high evaporation flux at Zhangye (Supplementary Figure S3). The results in Figure 10 are for the OLS regression. At high concentration gradients (> 200 ppm), the two methods gave similar linear

correlation coefficients with the Craig-Gordon model δ_E values (0.72 for FG and 0.66 for Keeling method with OLS), and the Keeling method with OLS had a higher RMSE (6.56‰) and a higher mean bias (0.81‰) than the FG method (6.03‰ RMSE, 0.65‰ MB). When the vapor gradient was smaller than 200 ppm in magnitude, both methods produced weaker correlation with the Craig-Gordon model results than when the gradient was larger, but the Keeling method with OLS slightly outperformed the FG method in terms of the RMSE (6.26‰ for Keeling and 7.68‰ for FG) and the mean bias (0.57‰ for Keeling and 2.61‰ for FG). If the YS regression was used, the Keeling mean bias and RMSE changed slightly to 1.76‰ and 6.83‰ at high concentration gradients and 3.03‰ and 6.95‰ at low concentration gradients, respectively (Figure S4).

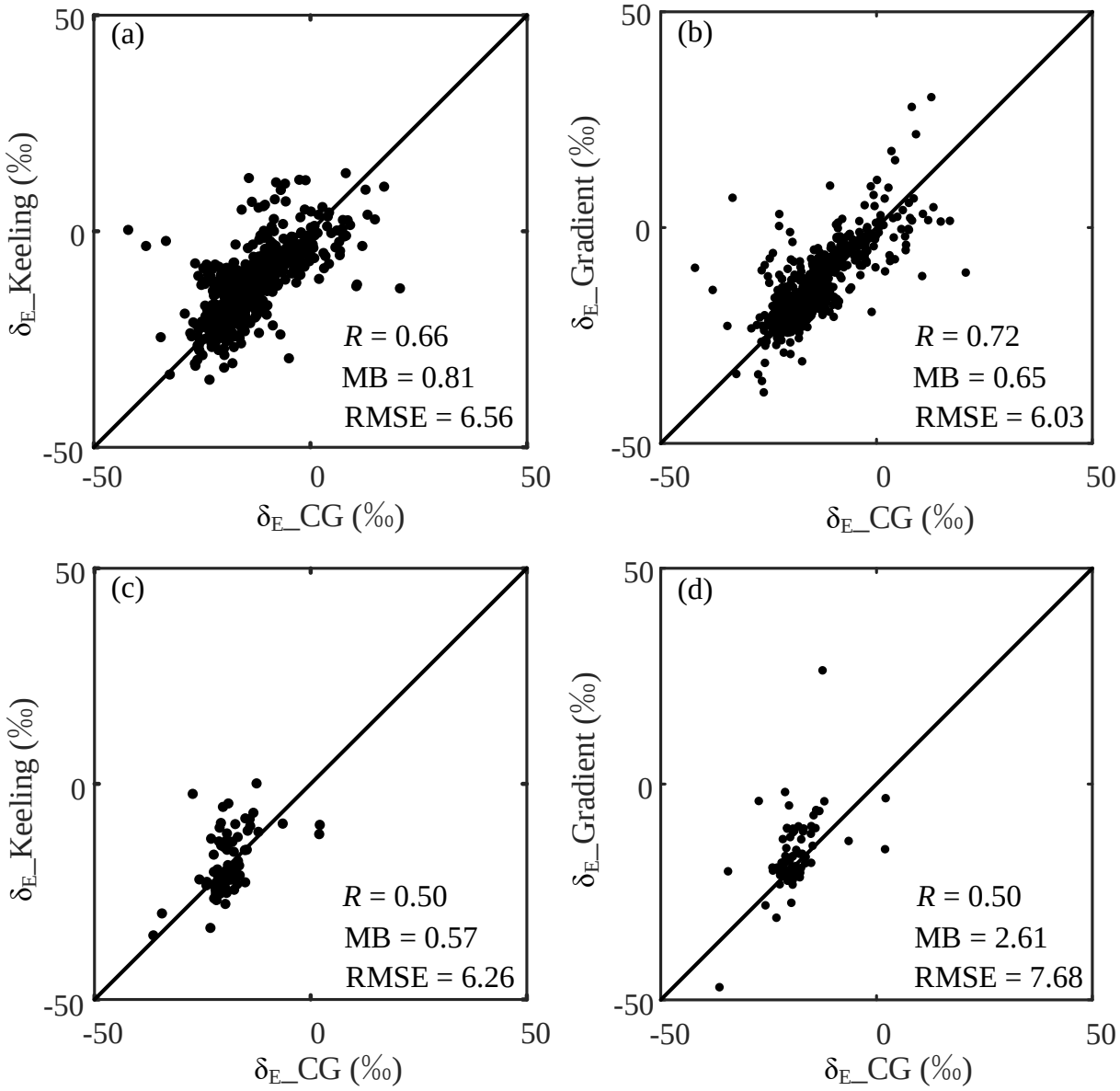

505

506 Figure 10. Comparison between the evaporation isotopic signature δ_E calculated by the Craig-
507 Gordon (CG) model with that from the Keeling method with the OLS regression and from the
508 FG method at Lake Taihu. Panels a and b: observations with hourly mean vertical concentration
509 difference greater than 200 ppm in magnitude; panels c and d: observations with hourly
510 concentration difference smaller than 200 ppm in magnitude.

511

512 The Keeling and the FG methods are mathematically equivalent and give identical δ_E if
513 the same hourly concentration and hourly water vapor δ at the two measurement heights are used
514 to determine δ_E (Good et al., 2012). In the present case, because the Keeling method used high-
515 frequency data collected at both heights, it was constrained by both temporal and vertical
516 variations. However, the FG was constrained only by vertical variations because it used the
517 hourly means. The results given in Figure 10 suggests that the Keeling method using high
518 frequency data may be more reliable at times of low vertical concentration gradient than the FG
519 method because it retains temporal variability.
520
521 The measurement systems at Zhangye and Lake Taihu both deployed buffer volumes to
522 help improve the hourly mean gradient measurements. These buffers had a time constant of
523 about 1 min, effectively damping out turbulent fluctuations at frequencies higher than about 0.02
524 Hz. Measurements taken at a frequency equivalent to the inverse of the instrument response time
525 and without physical or digital averaging (Griffis et al., 2007; Good et al., 2012) may further
526 improve the Keeling method under low vertical gradient conditions.
527
528 **4 Summary and Conclusions**
529 The error structures of the two IRIS analyzers (a Picarro and an LGR) were characterized as
530 functions of water vapor concentration. Both instruments showed smaller measurement errors in
531 more humid conditions. For the Picarro analyzer used at Zhangye, the correlation between
532 measurement errors in the inverse of the concentration and the water vapor δ was slightly
533 positive (about 0.09) at low concentrations (~10,000 ppm) and varied around zero at high

concentrations (~25,000 ppm). For the LGR analyzer used at Lake Taihu, the error correlation was mostly positive (about 0.14) and did not seem to depend on the vapor concentration.

The YS and the OLS regression method produced equally robust estimates of δ_E for the Zhangye cropland and for Lake Taihu, with the former giving a tighter standard error structure than the latter. The mean bias error was 0.92‰ and 1.06‰ for YS and 0.73‰ and 0.14‰ for OLS, at Zhangye and Lake Taihu, respectively. The GMR method was systematically biased high (8.10‰ and 21.44‰ at Zhangye and Lake Taihu, respectively) when the linear correlation *R* between the inverse of the vapor concentration and the vapor δ value was negative and biased low (-23.12‰ and -27.60‰ at Zhangye and Lake Taihu, respectively) when *R* was positive. The large GMR bias errors were attributed to the fact that the vapor δ measurement had relative errors that were 3 to 10 times as large as relative errors in the concentration measurement for the IRIS instruments used in this study.

Previous studies on ^{13}C showed that both the bias error and the random uncertainty of the Keeling intercept decrease with increasing concentration range. In the present study, increasing the water vapor concentration range reduced the standard error of the Keeling method using the YS and OLS regression, but had little effect on the bias error beyond the concentration range of about 200 ppm. On the other hand, the bias error was much smaller using two-height data (0.99‰ for YS and 0.44‰ for OLS, average of the two sites) than using one-height data (2.65‰ for YS and -0.34‰ for OLS) to perform the regression analysis.

556 The Keeling method with the OLS regression gave a slightly more robust estimate of δ_E
557 for Lake Taihu than the flux-gradient method under conditions of low vertical water vapor
558 concentration gradient, when compared with the Craig-Gordon model prediction. This result
559 requires further evaluation because it was based on a small sample size (82 hourly observations)
560 and because high frequency variations (frequency greater than about 0.02 Hz) were filtered out
561 by our measurement systems. A measurement system that samples the concentration and vapor
562 delta sequentially between two or more heights and at the true eddy time scales may yield better
563 results than shown in the present study.
564

565 **Acknowledgements**

566 The authors would like to thank all the participants of the experiments at Zhangye and at Taihu
567 Eddy Flux Network. This work was supported by the National Key R&D Program of China
568 (grant 2019YFA0607202), China Scholarship Council, the National Natural Science Foundation
569 of China (grant 41975143) and the U.S. National Science Foundation (grant 1520684). The water
570 vapor isotope data used in this study are available on the website https://vapor-isotope.yale.edu/.
571

572 **References**

573 Bowen, G. J., Cai, Z., Fiorella, R. P., & Putman, A. L. (2019). Isotopes in the water cycle:
574 Regional- to global-scale patterns and applications. *Annual Review of Earth and Planetary*
575 *Sciences*, *47*, 457–479. doi.org/10.1146/annurev-earth-053018
576 Bowling, D. R., Baldocchi, D. D., & Monson, R. K. (1999). Dynamics of isotopic exchange of
577 carbon dioxide in a tennessee deciduous forest. *Global Biogeochemical Cycles*, *13*(4), 903–
578 922. doi.org/10.1029/1999GB900072
579 Bowling, D. R., Burns, S. P., Conway, T. J., Monson, R. K., & White, J. W. C. (2005). Extensive
580 observations of CO_2 carbon isotope content in and above a high-elevation subalpine forest.

Global Biogeochemical Cycles, *19*(3). doi.org/10.1029/2004GB002394

Chen, C., Pang, J., Wei, J., Wen, X., & Sun, X. (2017). Inter-comparison of three models for $\delta^{13}C$ of respiration with four regression approaches. *Agricultural and Forest Meteorology*, *247*, 229–239. doi.org/10.1016/j.agrformet.2017.08.002

Craig, H., & Gordon, L. I. (1965). Deuterium and oxygen 18 variations in the ocean and the marine atmosphere. In E. Tongiorgi (Ed.), *Stable isotopes in oceanographic studies and paleotemperatures* (pp. 9–130). Pisa: Consiglio Nazionale Delle Ricerche Laboratorio di Geologia Nucleare.

Delattre, H., Vallet-Coulomb, C., & Sonzogni, C. (2015). Deuterium excess in the atmospheric water vapour of a Mediterranean coastal wetland: regional vs. local signatures. *Atmospheric Chemistry and Physics*, *15*, 10167–10181. doi.org/10.5194/acp-15-10167-2015

Dubbert, M., & Werner, C. (2019). Water fluxes mediated by vegetation: emerging isotopic insights at the soil and atmosphere interfaces. *New Phytologist*, *221*(4), 1754–1763. doi.org/10.1111/nph.15547

Fiorella, R. P., Poulsen, C. J., & Matheny, A. M. (2018). Seasonal patterns of water cycling in a deep, continental mountain valley inferred from stable water vapor isotopes. *Journal of Geophysical Research: Atmospheres*, *123*, 7271–7291. doi.org/10.1029/2017JD028093

Gat, J. R., Bowser, C. J., & Kendall, C. (1994). The contribution of evaporation from the Great Lakes to the continental atmosphere: estimate based on stable isotope data. *Geophysical Research Letters*, *21*(7), 557–560. doi.org/10.1029/94GL00069

Gibson, J. J., Edwards, T. W. D., Bursey, G. G., & Prowse, T. D. (1993). Estimating evaporation using stable isotopes. *Nordic Hydrology*, *24*, 79–94.

Good, S. P., Soderberg, K., Wang, L., & Caylor, K. K. (2012). Uncertainties in the assessment of

the isotopic composition of surface fluxes: A direct comparison of techniques using laser-based water vapor isotope analyzers. *Journal of Geophysical Research: Atmospheres*, *117*(D15). doi.org/10.1029/2011JD017168

Good, S. P., Soderberg, K., Guan, K., King, E. G., Scanlon, T. M., Caylor, K. K., et al. (2014). Seeking genericity in the selection of parameter sets: Impact on hydrological model efficiency. *Water Resources Research*, *50*, 1410–1432. doi.org/10.1002/2013WR014333

Good, S. P., Noone, D., & Bowen, G. (2015). Hydrologic connectivity constrains partitioning of global terrestrial water fluxes. *Science*, *349*(6244), 175–177. doi.org/10.1126/science.aaa5931

Griffis, T. J., Baker, J. M., Sargent, S. D., Tanner, B. D., & Zhang, J. (2004). Measuring field-scale isotopic CO_2 fluxes with tunable diode laser absorption spectroscopy and micrometeorological techniques. *Agricultural and Forest Meteorology*, *124*(1–2), 15–29. doi.org/10.1016/j.agrformet.2004.01.009

Griffis, T. J., Lee, X., Baker, J. M., Sargent, S. D., King, J. Y. (2005). Feasibility of quantifying ecosystem–atmosphere $C^{18}O^{16}O$ exchange using laser spectroscopy and the flux-gradient method, *Agricultural and Forest Meteorology*, *135*, 44–60, doi:10.1016/j.agrformet.2005.10.002

Griffis, T. J., Zhang, J., Baker, J. M., Kljun, N., & Billmark, K. (2007). Determining carbon isotope signatures from micrometeorological measurements: Implications for studying biosphere-atmosphere exchange processes. *Boundary-Layer Meteorology*, *123*(2), 295–316. doi.org/10.1007/s10546-006-9143-8

Griffis, T. J., Wood, J. D., Baker, J. M., Lee, X., Xiao, K., Chen, Z., et al. (2016). Investigating the source, transport, and isotope composition of water vapor in the planetary boundary

layer. *Atmospheric Chemistry and Physics*, *16*(8), 5139–5157. doi:10.5194/acp-16-5139-2016

Huang, L., & Wen, X. (2014). Temporal variations of atmospheric water vapor δD and $\delta^{18}O$ above an arid artificial oasis cropland in the Heihe River Basin. *Journal of Geophysical Research: Atmospheres*, *119*, 11456–11476. doi.org/10.1002/2014JD021891

Kayler, Z. E., Ganio, L., Hauck, M., Pypker, T. G., Sulzman, E. W., Mix, A. C., & Bond, B. J. (2010). Bias and uncertainty of $\delta^{13}CO_2$ isotopic mixing models. *Oecologia*, *163*(1), 227–234. doi.org/10.1007/s00442-009-1531-6

Keeling, D. C. (1958). The concentration and isotopic abundances of atmospheric carbon dioxide in rural areas. *Geochimica et Cosmochimica Acta*, *13*(4), 322–334.

Kermack, A. K. A., & Haldane, J. B. S. (1950). Organic correlation and allometry. *Biometrika*, *37*(1), 30–41.

Lee, X., Kim, K., & Smith, R. (2007). Temporal variations of the $^{18}O/^{16}O$ signal of the whole-canopy transpiration in a temperate forest. *Global Biogeochemical Cycles*, *21*(3). doi.org/10.1029/2006GB002871

Lee, X., Huang, J., & Patton, E. G. (2012). A large-eddy simulation study of water vapour and carbon dioxide isotopes in the atmospheric boundary layer. *Boundary-Layer Meteorology*, *145*(1), 229–248. doi.org/10.1007/s10546-011-9631-3

Lee, X., Liu, S., Xiao, W., Wang, W., Gao, Z., Cao, C., et al. (2014). The Taihu Eddy Flux Network: An observational program on energy, water, and greenhouse gas fluxes of a large freshwater lake. *Bulletin of the American Meteorological Society*, *95*(10), 1583–1594. doi.org/10.1175/BAMS-D-13-00136.1

Lu, X., Liang, L. L., Wang, L., Jenerette, G. D., McCabe, M. F., & Grantz, D. A. (2017).

Partitioning of evapotranspiration using a stable isotope technique in an arid and high temperature agricultural production system. *Agricultural Water Management*, *179*, 103–109. doi.org/10.1016/j.agwat.2016.08.012

Miller, J. B., & Tans, P. P. (2003). Calculating isotopic fractionation from atmospheric measurements at various scales. *Tellus, Series B: Chemical and Physical Meteorology*, *55*(2), 207–214. doi.org/10.1034/j.1600-0889.2003.00020.x

Ogée, J., Peylin, P., Ciais, P., Bariac, T., Brunet, Y., Berbigier, P., et al. (2003). Partitioning net ecosystem carbon exchange into net assimilation and respiration using $^{13}CO_2$ measurements: A cost-effective sampling strategy. *Global Biogeochemical Cycles*, *17*(2). doi.org/10.1029/2002gb001995

Pataki, D. E., Ehleringer, J. R., Flanagan, L. B., Yakir, D., Bowling, D. R., Still, C. J., et al. (2003). The application and interpretation of Keeling plots in terrestrial carbon cycle research. *Global Biogeochemical Cycles*, *17*(1). doi.org/10.1029/2001GB001850

Quade, M., Klosterhalfen, A., Graf, A., Brüggemann, N., Hermes, N., Vereecken, H., & Rothfuss, Y. (2019). In-situ monitoring of soil water isotopic composition for partitioning of evapotranspiration during one growing season of sugar beet (Beta vulgaris). *Agricultural and Forest Meteorology*, *266–267*, 53–64. doi.org/10.1016/j.agrformet.2018.12.002

Simonin, K. A., Link, P., Rempe, D., Miller, S., Oshun, J., Bode, C., et al. (2014). Vegetation induced changes in the stable isotope composition of near surface humidity. *Ecohydrology*, *7*(3), 936–949. doi.org/10.1002/eco.1420

Sun, X., Wilcox, B. P., & Zou, C. B. (2019). Evapotranspiration partitioning in dryland ecosystems: A global meta-analysis of in situ studies. *Journal of Hydrology*, *576*, 123–136. doi.org/10.1016/j.jhydrol.2019.06.022

673 Unger, S., Máguas, C., Pereira, J. S., Aires, L. M., David, T. S., & Werner, C. (2010).
674 Disentangling drought-induced variation in ecosystem and soil respiration using stable
675 carbon isotopes. *Oecologia*, *163*(4), 1043–1057. doi.org/10.1007/s00442-010-1576-6
676 Vardag, S. N., Hammer, S., & Levin, I. (2016). Evaluation of 4 years of continuous $\delta^{13}C(CO_2)$
677 data using a moving Keeling plot method. *Biogeosciences*, *13*(14), 4237–4251.
678 doi.org/10.5194/bg-13-4237-2016
679 Wang, S., Zhang, M., Che, Y., Chen, F., & Qiang, F. (2016). Contribution of recycled moisture to
680 precipitation in oases of arid central Asia: A stable isotope approach. *Water Resources*
681 *Research*, *52*, 3246–3257. doi.org/10.1111/j.1752-1688.1969.tb04897.x
682 Wehr, R., Munger, J. W., Nelson, D. D., McManus, J. B., Zahniser,M. S., Davdison, E. A.,Wofsy,
683 S. C., & Saleska, S. R. (2016). Seasonality of temperate forest photosynthesis and daytime
684 respiration, *Nature*, *534*, 680–683, doi:10.1038/nature17966
685 Wehr, R., & Saleska, S. R. (2017). The long-solved problem of the best-fit straight line:
686 Application to isotopic mixing lines. *Biogeosciences*, *14*(1), 17–29. doi.org/10.5194/bg-14-
687 17-2017
688 Wei, Z., Lee, X., Wen, X., & Xiao, W. (2018). Evapotranspiration partitioning for three agro-
689 ecosystems with contrasting moisture conditions: A comparison of an isotope method and a
690 two-source model calculation. *Agricultural and Forest Meteorology*, *252*, 296–310.
691 doi.org/10.1016/j.agrformet.2018.01.019
692 Wei, Z., Lee, X., Aemisegger, F., Benetti, M., Berkelhammer, M., Casado, M., et al. (2019). A
693 global database of water vapor isotopes measured with high temporal resolution infrared
694 laser spectroscopy. *Scientific Data*, *6*, 180302. doi.org/10.1038/sdata.2018.302
695 Welp, L. R., Lee, X., Kim, K., Griffis, T. J., Billmark, K. A., & Baker, J. M. (2008). $\delta^{18}O$ of

696 water vapour, evapotranspiration and the sites of leaf water evaporation in a soybean
697 canopy. *Plant, Cell and Environment*, *31*(9), 1214–1228. doi.org/10.1111/j.1365-
698 3040.2008.01826.x
699 Welp, L. R., Lee, X., Griffis, T. J., Wen, X. F., Xiao, W., Li, S., et al. (2012). A meta-analysis of
700 water vapor deuterium-excess in the midlatitude atmospheric surface layer. *Global*
701 *Biogeochemical Cycles*, *26*(3). doi.org/10.1029/2011GB004246
702 Wen, X., Sun, X., Zhang, S., Yu, G., Sargent, S. D., & Lee, X. (2008). Continuous measurement
703 of water vapor D/H and $^{18}O/^{16}O$ isotope ratios in the atmosphere. *Journal of Hydrology*,
704 *349*(3–4), 489–500. doi.org/10.1016/j.jhydrol.2007.11.021
705 Wen, X., Lee, X., Sun, X., Wang, J., Hu, Z., Li, S., & Yu, G. (2012a). Dew water isotopic ratios
706 and their relationships to ecosystem water pools and fluxes in a cropland and a grassland in
707 China. *Oecologia*, *168*(2), 549–561. doi.org/10.1007/s00442-011-2091-0
708 Wen, X., Lee, X., Sun, X., Wang, J., Tang, Y., Li, S., & Yu, G. (2012b). Intercomparison of four
709 commercial analyzers for water vapor isotope measurement. *Journal of Atmospheric and*
710 *Oceanic Technology*, *29*(2), 235–247. doi.org/10.1175/JTECH-D-10-05037.1
711 Wen, X., Yang, B., Sun, X., & Lee, X. (2016). Evapotranspiration partitioning through in-situ
712 oxygen isotope measurements in an oasis cropland. *Agricultural and Forest Meteorology*,
713 *230–231*, 89–96. doi.org/10.1016/j.agrformet.2015.12.003
714 Xiao, W., Lee, X., Hu, Y., Liu, S., Wang, W., Wen, X., et al. (2017). An experimental
715 investigation of kinetic fractionation of open-water evaporation over a large lake. *Journal of*
716 *Geophysical Research: Atmospheres*, *122*(21), 11,651–11,663.
717 doi.org/10.1002/2017JD026774
718 Xiao, W., Qian, Y., Lee, X., Wang, W., Zhang, M., Wen, X., et al. (2018). Hydrologic

719 implications of the isotopic kinetic fractionation of open-water evaporation. *Science China*
720 *Earth Sciences*, *61*(10), 1523–1532. doi.org/10.1007/s11430-018-9246-9
721 Yao, T., Zhang, X., Guan, H., Zhou, H., Hua, M., & Wang, X. (2018). Climatic and
722 environmental controls on stable isotopes in atmospheric water vapor near the surface
723 observed in Changsha, China. *Atmospheric Environment*, *189*, 252–263.
724 doi.org/10.1016/j.atmosenv.2018.07.008
725 Yepez, E. A., Williams, D. G., Scott, R. L., & Lin, G. (2003). Partitioning overstory and
726 understory evapotranspiration in a semiarid savanna woodland from the isotopic
727 composition of water vapor. *Agricultural and Forest Meteorology*, *119*(1–2), 53–68.
728 doi.org/10.1016/S0168-1923(03)00116-3
729 Yepez, E. A., Huxman, T. E., Ignace, D. D., English, N. B., Weltzin, J. F., Castellanos, A. E., &
730 Williams, D. G. (2005). Dynamics of transpiration and evaporation following a moisture
731 pulse in semiarid grassland: A chamber-based isotope method for partitioning flux
732 components. *Agricultural and Forest Meteorology*, *132*(3–4), 359–376.
733 doi.org/10.1016/j.agrformet.2005.09.006
734 York, D. (1966). Least-squares fitting of a straight line. *Canandian Journal of Physics*, *44*, 1079–
735 1086.
736 York, D. (1969). Least squares fitting of a straight line with correlated errors. *Earth and*
737 *Planetary Science Letters*, *5*, 320–324.
738 York, D., Evensen, N. M., Martínez, M. L., & De Basabe Delgado, J. (2004). Unified equations
739 for the slope, intercept, and standard errors of the best straight line. *American Journal of*
740 *Physics*, *72*(3), 367–375. doi.org/10.1119/1.1632486
741 Zannoni, D., Steen-Larsen, H. C., Stenni, B., Dreossi, G., & Rampazzo, G. (2019a). Synoptic to

742 mesoscale processes affecting the water vapor isotopic daily cycle over a coastal lagoon.
743 *Atmospheric Environment*, *197*, 118–130. doi.org/10.1016/j.atmosenv.2018.10.032
744 Zannoni, D., Steen-Larsen, H. C., Rampazzo, G., Dreossi, G., Stenni, B., & Bergamasco, A.
745 (2019b). The atmospheric water cycle of a coastal lagoon: An isotope study of the
746 interactions between water vapor, precipitation and surface waters. *Journal of Hydrology*,
747 *572*, 630–644. doi.org/10.1016/j.jhydrol.2019.03.033
748 Zobitz, J. M., Keener, J. P., Schnyder, H., & Bowling, D. R. (2006). Sensitivity analysis and
749 quantification of uncertainty for isotopic mixing relationships in carbon cycle research.
750 *Agricultural and Forest Meteorology*, *136*(1–2), 56–75.
751 doi.org/10.1016/j.agrformet.2006.01.003
752